Discovery of Potent and Selective Inhibitors of Ataxia Telangiectasia Mutated and Rad3 Related (ATR) Protein Kinase as Potential Anticancer Agents

14 AUTHORS, INCLUDING:

Ronald Knegtel
Vertex Pharmaceuticals (Europe) Ltd
53 PUBLICATIONS   **1,735** CITATIONS

SEE PROFILE

Somhairle Maccormick
University of Antwerp
**12** PUBLICATIONS   **319** CITATIONS

SEE PROFILE

Discovery of Potent and Selective Inhibitors of Ataxia Telangiectasia Mutated and Rad3 Related (ATR) Protein Kinase as Potential Anticancer Agents

Jean-Damien Charrier,[†] Steven J. Durrant,[†] Julian M. C. Golec,[†] David P. Kay,[†] Ronald M. A. Knegtel,[†] Somhairle MacCormick,[†] Michael Mortimore,[†] Michael E. O'Donnell,[†] Joanne L. Pinder,[†] Philip M. Reaper,[‡] Alistair P. Rutherford,[†] Paul S. H. Wang,[‡] Stephen C. Young,[†] and John R. Pollard*,[‡]

[†]Chemistry Department and [‡]Biology Department, Vertex Pharmaceuticals (Europe) Ltd., 88 Milton Park, Abingdon, Oxfordshire OX14 4RY, United Kingdom

S *Supporting Information*

ABSTRACT: DNA-damaging agents are among the most frequently used anticancer drugs. However, they provide only modest benefit in most cancers. This may be attributed to a genome maintenance network, the DNA damage response (DDR), that recognizes and repairs damaged DNA. ATR is a major regulator of the DDR and an attractive anticancer target. Herein, we describe the discovery of a series of aminopyrazines with potent and selective ATR inhibition. Compound **45** inhibits ATR with a K_i of 6 nM, shows >600-fold selectivity over related kinases ATM or DNA-PK, and blocks ATR signaling in cells with an IC_{50} of 0.42 μM. Using this compound, we show that ATR inhibition markedly enhances death induced by DNA-damaging agents in certain cancers but not normal cells. This differential response between cancer and normal cells highlights the great potential for ATR inhibition as a novel mechanism to dramatically increase the efficacy of many established drugs and ionizing radiation.

45
K_i (ATR) = 6nM
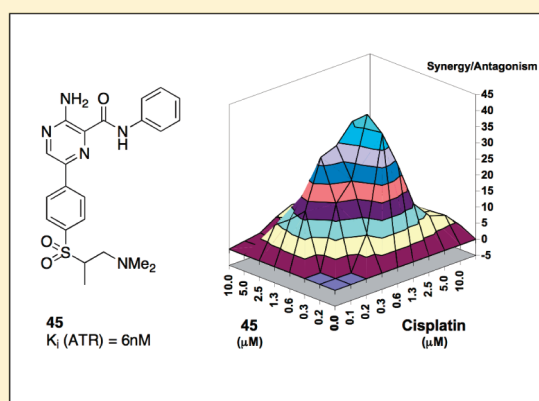
INTRODUCTION

DNA-damaging agents such as cisplatin, irinotecan, gemcitabine, and ionizing radiation (IR) represent the cornerstone for the treatment of solid tumors. While they can be highly effective in the treatment of certain cancers, for example, testicular cancer,[1] for the majority of solid tumors, they provide only modest benefit. The fact that, in tumor cells, proficient processes exist to repair the damaged DNA[2−5] provides one explanation for the poor response. Important among these processes is the DNA damage response (DDR).[6] Two phosphoinositol 3-kinase-like kinase (PIKK) family members, ATM (ataxia telangiectasia mutated) and ATR (ATM and Rad-3 related), act together as apical regulators of this signaling pathway.[7,8] Between them, they act on a complex network involving hundreds of substrates, many of which are shared, to regulate a wide range of critical functions such as cell cycle checkpoint activation and DNA damage repair. Although ATM and ATR are recruited to different DNA strand break structures, it is now known that these structures can be readily interconverted in the cell.[8] Loss of ATM function is very common in tumors, either through loss of ATM itself or through defects in upstream and downstream signaling.[9−12] It is believed that such a loss enables the proliferation of incipient cancer cells that carry DNA lesions.[13] While this may confer a growth advantage on the tumor cells, it is likely to place more reliance

on the ATR pathway, for survival following DNA damage. In support of this, some studies have shown that disruption of p53 function, a major substrate for ATM, enhances cell sensitivity to ATR disruption.[14,15] The exploitation of a potentially synthetic lethal interaction between the ATR and the ATM-p53 pathway provides an attractive opportunity to deliver anticancer drugs that increase the efficacy of established DNA-damaging agents. The benefits of exploiting such synthetic lethal interactions have recently been demonstrated with inhibitors of poly-ADP-ribose polymerase (PARP), an enzyme also involved in DNA repair.[16] Cancer cells defective in the breast cancer susceptibility proteins BRCA1/2, which participate in a complementary DNA repair pathway, are acutely sensitive to inhibitors of PARP. A number of PARP inhibitors are in clinical trials, and initial results are highly encouraging.[17,18]

A number of potent and selective inhibitors of the PIKK family members ATM (e.g. **1**, KU-55933[19]), DNA-PK(e.g. **2**, NU-7026[20]), and the ATR substrate Chk**1** (e.g. **3**, AZD-7762[21]) have been disclosed. In contrast, reported inhibitors of ATR such as **4** (caffeine[22]) and **5** (schisandrin B[23]) (Figure 1) are weak and nonselective (Table 1). However, there is a growing interest in
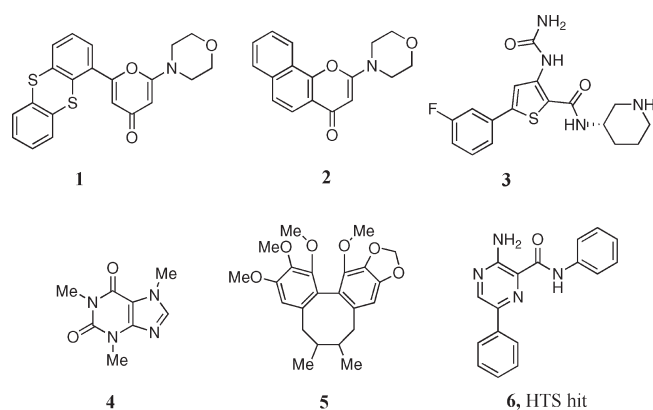
Figure 1. Structures of selected inhibitors of the DDR.

Table 1. Inhibitory Activity (μM) of 1, 2, 4, and 5 against PIKK Family Members

	IC$_{50}$ (μM)			
	1	**2**	**4**	**5**
ATR	>100	>100	1100	7.2
ATM	0.013	>100	200	1740
DNAPK	2.5	0.23	10000	>10^6
mTor	9.3	6.4	400	n/a

ATR as a target for anticancer drugs,[24] and a number of patent applications have recently been filed that claim ATR inhibitors (from AstraZeneca and Vertex), although limited biochemical or cellular data are disclosed in these documents.[25−27] The work described here rectifies the shortage of good, well-characterized chemical tools that has hampered characterization of ATR as an oncology target.[24] Specifically, these compounds will be valuable in helping to define the potential for synthetic lethal interactions with the ATM signaling pathway and the impact of ATR inhibition on normal cells.

We report a novel series of 3-amino-6-arylpyrazines that has provided potent and highly selective inhibitors of ATR. Starting from the hit compound **6** (Figure 1), identified from a high-throughput screen (HTS), a combination of structure−activity relationship (SAR) studies and homology modeling led to an understanding of the interactions between the inhibitors and the ATR active site that are critical for both potency and selectivity. Compound **45** represents one of the most potent (K_{iapp} of 6 nM for ATR) and selective members of the series and is used here to illustrate the attractive cellular phenotype that can be achieved by inhibiting ATR.

■ CHEMISTRY

Compound **8**, with its 6-bromo functional group, provided a late stage intermediate that enabled rapid and versatile modification of the phenyl ring at the 6-position of the pyrazine nucleus in compound **6**. The synthetic route for the preparation of ATR inhibitors **6−47** is depicted in Scheme 1. Commercial methyl aminopyrazin-2-carboxylate **53** was brominated at the 6-position of the pyrazine nucleus with NBS,[28] to provide intermediate **54** in high yield. Base hydrolysis of the methyl ester **54** afforded the carboxylic acid **56**, which condensed with aniline to give the desired advanced intermediate amide **8**.[29] Diversity of the group at the 6-position of the pyrazine ring was introduced when **8** was subjected to Suzuki cross-coupling[30] reactions with a range of boronic acids/boronates to generate inhibitors **6** and **10−47**. The fully saturated cyclohexane **9** was produced from the cyclohexene derivative **10** by reduction under hydrogenation conditions.[31]

For alternative amides at the 2-position of the pyrazine core (e.g., cyclohexylamide **48**), the chemical sequence described in Scheme 2 was used. A Suzuki cross-coupling reaction between 4-(methylsulfonyl)phenylboronic acid and **54** provided advanced intermediate **57**, which in turn was converted to amide **48**. An array of bicyclic heteroaryl moieties that could act as

phenylamide isosteres was also prepared (benzimidazole, benzoxazole, benzothiazole, and indoles **49−52**; Schemes 3 and 4). Early installation of the bicyclic heteroaryl feature preserved the versatility of the 6-position. Thus, treatment of intermediate carboxylic acid **56** with phenylenediamine in DME, in the presence of diethoxy-phosphorylformonitrile, afforded the late stage intermediate benzimidazole **58** in moderate yield.[32] Subsequent coupling with 4-(methylsulfonyl) phenylboronic acid provided isostere **49**. A similar functionalization sequence was adopted for the synthesis of benzoxazole and benzothiazole isosteres **50** and **51**. Conversion of the nitrile **59** into late stage intermediates benzoxazole **60** or benzothiazole **61** proceeded with 2-aminophenol or 2-aminothiophenol in moderate yield.[33−35] Suzuki cross-coupling with 4-(methylsulfonyl)boronic acid gave the required isosteres **50** and **51**.

Although the chemical sequences described in Scheme 3 for the preparation of isosteres **49−51** have provided the desired compounds, the reverse syntheses (i.e., functionalization through Suzuki cross-coupling prior to the construction of the isosteric motifs, in a sequence similar to that described in Scheme 2) have also been successfully utilized and are preferred for exploration of the substitution of the bicyclic isosteres.

A sequential derivatization (Scheme 4) of building block **62**[36] provided the indole variant **52**. This sequence enabled the introduction of the indole motif at the most reactive position (vicinal to amino group), using N-Boc-indol-2-ylboronic ester in a palladium catalyzed cross-coupling reaction; a second Suzuki coupling with 4-(methylsulfonyl)phenylboronic acid, followed by Boc deprotection with TFA, afforded the desired indole containing derivative **52**.

■ RESULTS AND DISCUSSION

Compound **6** was identified from a HTS against full-length recombinant ATR. It inhibits ATR with an IC$_{50}$ of 0.62 μM and has good selectivity against ATM and DNAPK (IC$_{50}$ > 8 μM). However, inhibition of ATR activity in cell-based assays, as measured by a reduction in hydroxyurea-induced phosphorylation of H2AX, a direct substrate of ATR [37] was not observed (IC$_{50}$ > 2.5 μM). Because high-resolution crystallographic data for any member of the PIKK family were unavailable, the related kinase phosphatidylinositol 3-kinase γ (PI3K-γ) was used as a structural template[38,39] for an ATR homology model to aid inhibitor design. To provide guidance on selectivity, homology models of ATM and DNAPK were also constructed from the same root. The low-resolution structure of DNAPK reported by Sibanda et al.[40] was used to provide guidance on the overall fold. Although sequence identity between PI3K-γ and PIKK family members is relatively low (e.g., 22% between PI3K-γ and ATR in the kinase domain), a number of important residues are conserved within the active site. These include a salt bridge

Scheme 1[a]
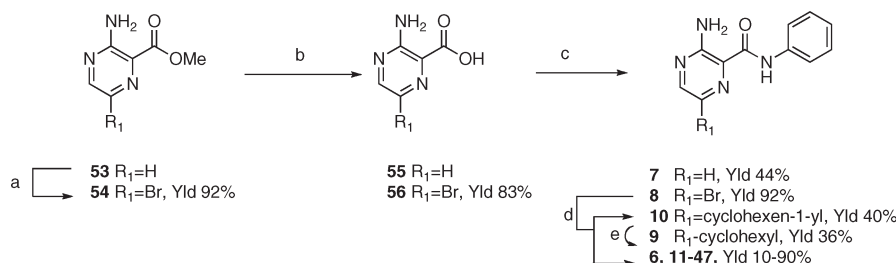
[a] Reagents and conditions: (a) NBS, MeCN, RT, 18 h, 92%. (b) LiOH, MeOH:H$_2$O (1:1), reflux 2 h, 83%. (c) CDI, DIPEA, aniline, DMAP, DMSO, RT, 18 h, 44−92%. (d) Boronic acid, Na$_2$CO$_3$, PdCl$_2$(PPh$_3$)$_2$, DMF:H$_2$O (2:1), 88 °C, 18 h, 10−90%. (e) H-cube, H$_2$, Pd/C (cat cart), EtOH, 36%.

(Asp2494 and Lys2327 in ATR) and the Tyr2365 gatekeeper residue, which, together, helped refine the local alignment within the active site.

The homology model with the HTS hit **6** bound to ATR is shown in Figure 2. The positioning of compound **6** in the model active site was guided by a co-complex structure of a related aminopyrazine in PI3K-γ (not shown). This enabled us to locate critical H-bond interactions between the hinge motif of the protein active site and the core scaffold. Minimization of the co-complex of **6** with ATR predicts H-bond interactions of the ring sp^2-nitrogen with the backbone −NH− of Val2378 (3.01 Å) and the exocyclic amine of the amino-pyrazine with the carbonyl of Glu2380 (3.08 Å). The biaryl motif of the inhibitor is also anticipated to contribute to the binding through π-stacking with the indole ring of Trp2379.

The hydroxyl of the gatekeeper residue (Tyr2365 in ATR) is located near the amide carbonyl at the 2-position of the pyrazine and appears to be positioned to form a H-bond. A salt bridge between Asp2494 and Lys2327, conserved across the PIKK family, is predicted to be disrupted by the aniline ring of inhibitor **6**, forcing the side chain of Asp2494 down, thus allowing the aromatic ring to fit under the P loop (Figure 2). This P loop, unusually rich in lipophilic residues when compared with most kinases, appears to fold over the aniline ring at the 2-position (Figure 3) and may also contribute to lipophilic binding.

In addition to the interactions described above, the potential interactions between compound **6** and ATM or DNAPK were also examined (described in detail below). This work suggested exploitable differences that should allow selectivity against these related kinases to be engineered.

With the objective of increasing potency while preserving selectivity, a first round of exploration was conducted through modification or substitution of the 6-aryl ring (Table 2). As predicted by the homology model, the π-stacking interaction between the 6-aryl in **6** and the Trp2379 makes an important contribution to the potency of the inhibitor. Removal of the phenyl ring (**7** and **8**) resulted in a 10-fold loss of binding affinity, and its complete or partial reduction (cyclohexyl **9** and cyclohexenyl **10**, respectively) led to about 5-fold decrease in potency. These results prompted us to retain an aromatic group at the 6-position of the aminopyrazine core. Exchanging the 6-phenyl group with a pyridine (**11**) produced 3-fold potency increase. However, inhibition of some Cyp isoforms was also increased (e.g., IC$_{50}$ $_{cyp3A4}$ 2 μM for **11** vs IC$_{50}$ $_{cyp3A4}$ >100 μM for **6**), discouraging us from using this motif further.

Compounds **13−19** provided information on the effects of substitution at the ortho-position. Introduction of a nitrile group

Scheme 2[a]
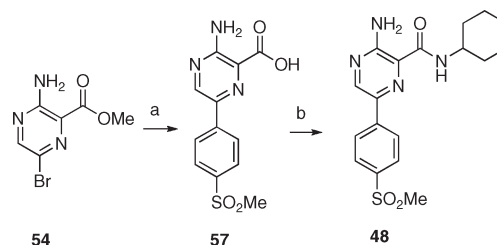
[a] Reagents and conditions: (a) 4-(Methylsulfonyl) phenylboronic acid, Na$_2$CO$_3$, PdCl$_2$(PPh$_3$)$_2$, DME, 90 °C, 9 h, 91%. (b) Diethoxy-phosphorylformonitrile, DIPEA, cyclohexylamine, DME, 88 °C, 10 min, microwave, 69%.

Scheme 3[a]
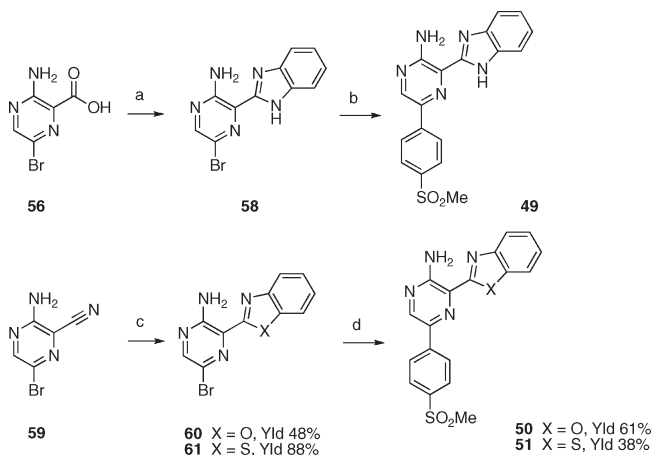
[a] Reagents and conditions: (a) Diethoxy-phosphorylformonitrile, phenylenediamine, Et$_3$N, DME, 170 °C, 20 min, microwave, 43%. (b) 4-(Methylsulfonyl)phenylboronic acid, Na$_2$CO$_3$, PdCl$_2$(PPh$_3$)$_2$, DME, 150 °C, 3 h, microwave, 48%. (c) 2-Aminophenol or 2-aminothiophenol, DME, microwave 150 °C, 60 min, 48−88%. (d) 4-(Methylsulfonyl)phenylboronic acid, Na$_2$CO$_3$, Pd(PPh$_3$)$_4$, dioxane, 110 °C, 30 min, microwave, 38−61%.

(**13**) led to a 25-fold improvement in potency against ATR but also increased affinity for ATM and DNAPK. The enhanced potency for ATR and DNAPK can be explained by the possible formation of a new H-bond with a serine residue (Ser2305 in ATR or Ser3731 in DNAPK). Although ATM has no such serine

Scheme 4[a]
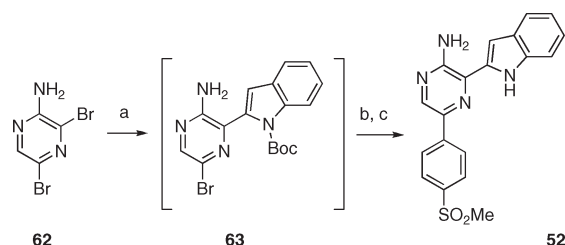
[a] Reagents and conditions: (a) N-Boc-indole-2-boronate, 2 M NaHCO₃, Pd(PPh₃)₄, DME, 120 °C, 10 min, microwave. (b) Then 4-(methylsulfonyl)phenylboronic acid, 120 °C, 10 min, microwave. (c) Then TFA:CH₂Cl₂ (1:1), RT, 15 h, 27% over three steps.
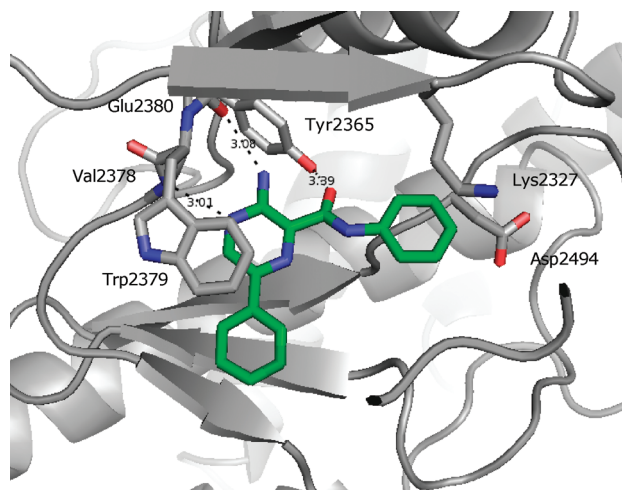

Figure 2. Cartoon representation of the ATR kinase domain homology model in complex with compound **6** (green). Selected aminoacids are highlighted as sticks.

residue, a slight change in conformation of the P loop could, in this case, allow a backbone N—H to participate in an H-bond to the nitrile group. No other substituent gave such affinity enhancement, although sulfoxide **14** was able to provide a 5-fold improvement.

Small group substitutions in the meta-position (compounds **20**−**25**) did not lead to significantly increased ATR potency, although selectivity was compromised by polar groups. On the other hand, substitution in the para-position (compounds **26**−**31**) led to the most potent and selective inhibitors in this array. The sulfone **27**, and to a lesser extent nitrile **26**, provided significant improvements in potency against ATR (25-fold for **27**), while retaining >100-fold selectivity against ATM and DNAPK (e.g., for **27**, $IC_{50\ ATR}$ = 26 nM, $IC_{50\ ATM}$ = >8 μM, and $IC_{50DNAPK}$ = 4.4 μM). These results can be attributed to the formation of a putative H-bond with the backbone N—H of the ATR-specific glycine residue (Gly2385), located C-terminal to the hinge region (Figure 3, blue van der Waals spheres). In ATM, this residue is a proline (Figure 3, red mesh), and no such H-bond can be formed. The equivalent residue in DNAPK is a threonine (Figure 3, yellow mesh), and any chance of a similar H-bond is likely to be blocked by the presence of the threonine side chain. Anilides **6**−**31** have the potential to form anilines In Vivo and so present a potential toxicological liability. Therefore, the effects of removing the anilide by reduction of the
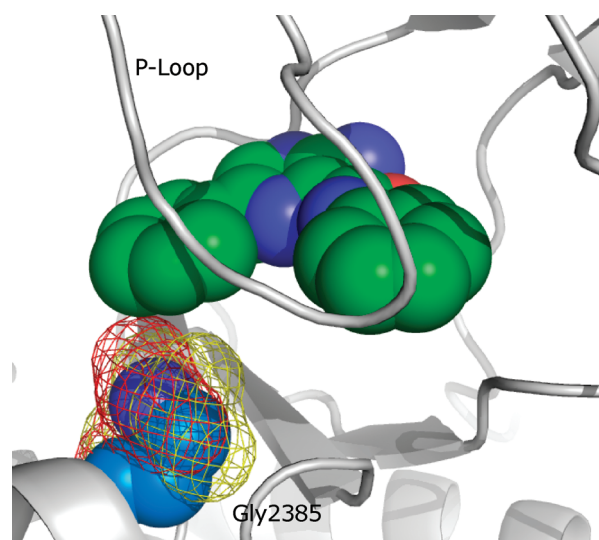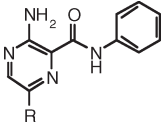

Figure 3. Cartoon representation of the ATR homology model in complex with compound **6** (green spheres). ATR-specific Gly2385 is represented in blue spheres; the corresponding residues in ATM and DNAPK are represented in mesh (Pro, red; Thr, yellow, respectively).

aromatic ring or by providing isosteres of the amide functional group were examined (compounds **48**−**52**). Saturation of the aniline ring (**48**) resulted in a >100-fold loss in potency. On the other hand, the use of heterocyclic motifs as anilide "isosteres" gave much better results. Benzimidazole **49**,[41] and by shape analogy benzoxazole **50**, benzothiazole **51**, and indole **52** show similar inhibitory activity to anilide **27** (Table 3) despite the fact only benzimidazole **49** has the potential to form the same H-bonds as the original amide. Neither replacement of the H-bond donor N—H in **27** with an oxygen acceptor in benzoxazole **50** nor removal of the H-bond acceptor carbonyl in indole **52** compromised potency. These results indicate that the proposed H-bond between the anilide carbonyl and the Tyr2365 is not a major contributor to binding, and we concluded that the amide group functions primarily as a linker to position the aromatic group under the P loop.

Although these bicyclic heteroaryls led to good ATR inhibition, selectivity against ATM was compromised in all cases. Compounds **49**−**52** cannot mimic the exact shape of the anilide in **27** and, as a consequence, have to bind deeper in the active site and become more likely to clash with the conserved tyrosine in the back of the adenosine-5′-triphosphate (ATP) binding pocket. Inspection of the homology models led us to hypothesize that the loss in selectivity may be associated with compounds **49**−**52** attaining a slightly different position in the active site relative to **27** (clockwise rotation illustrated in Figure 4). In this binding mode, compounds **49**−**52** avoid a clash with the tyrosine gatekeeper residue and also appear to alleviate a potential clash between the para-sulfone and Pro2775 in ATM that is observed for **27** (the equivalent residue is Gly2385 in ATR and Thr3809 in DNAPK). In addition, the ATM homology model predicts that an arginine residue (Arg2691) may also contribute to the enhanced potency through a H-bond with the sulfone in compounds **49**−**52**.
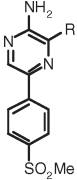
Because the anilide **27** remained the most potent and selective compound, it was chosen as the platform from which to further understand the interaction of the sulfone group. SARs between compounds in Table 2 and the ATR homology model (Figure 3)

Table 2. Structures and Inhibitory Activities of Compounds 6−31 against Selected Members of the PIKK Family

compd	R	enzyme inhibition IC$_{50}$ (μM)		
		ATR	ATM	DNAPK
6	−C$_6$H$_5$	0.62	>8	>8
7	−H	7.1	>8	>8
8	−Br	5.2	>8	>8
9	−cyclohexyl	3.0	>8	>8
10	−cyclohexen-1-yl	2.1	>8	>8
11	−pyrid-3-yl	0.18	>8	>8
12	−pyrid-4-yl	0.64	>8	5.0
13	−C$_6$H$_4$-2-CN	0.024	0.32	0.72
14	−C$_6$H$_4$-2-SOMe	0.13	3.0	2.0
15	−C$_6$H$_4$-2-SO$_2$Me	1.3	>8	>8
16	−C$_6$H$_4$-2-OH	2.4	>8	>8
17	−C$_6$H$_4$-2-OMe	0.74	>8	>8
18	−C$_6$H$_4$-2-Cl	0.70	>8	3.8
19	−C$_6$H$_4$-2-Me	1.4	>8	1.4
20	−C$_6$H$_4$-3-CN	0.40	>8	2.2
21	−C$_6$H$_4$-3-SO$_2$Me	0.34	6.6	0.74
22	−C$_6$H$_4$-3-OH	0.54	>8	2.2
23	−C$_6$H$_4$-3-OMe	2.2	>8	4.2
24	−C$_6$H$_4$-3-Cl	1.6	>8	>8
25	−C$_6$H$_4$-3-Me	0.56	>8	>8
26	−C$_6$H$_4$-4-CN	0.18	>8	>8
27	−C$_6$H$_4$-4-SO$_2$Me	0.026	>8	4.4
28	−C$_6$H$_4$-4-OH	0.32	5.8	1.8
29	−C$_6$H$_4$-4-OMe	1.5	>8	6.6
30	−C$_6$H$_4$-4-Cl	2.4	>8	>8
31	−C$_6$H$_4$-4-Me	1.7	>8	>8

Table 3. Structures and Inhibitory Activities of Compounds 27 and 48−52 against the PIKK Family

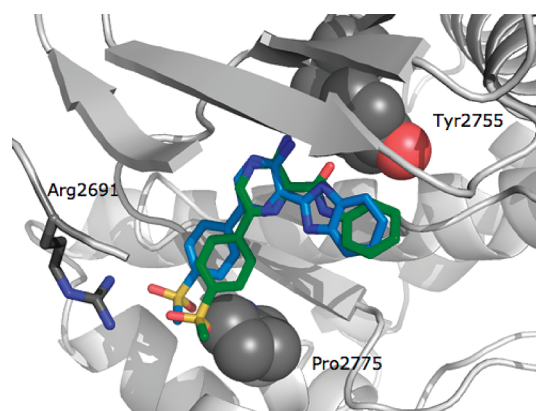| Compds	R	ATR Enz. inhibition IC$_{50}$ (μM)	ATM Enz. inhibition IC$_{50}$ (μM)	DNAPK Enz inhibition IC$_{50}$ (μM)
27		0.026	>8	4.3
48		3.56	>8	>8
49		0.030	0.38	2.1
50		0.036	0.84	1.4
51		0.022	0.72	2.9
52		0.023	0.12	2.4

Figure 4. Cartoon representation of the ATM homology model in complex with phenyl amide **27** (green) and benzimidazole isostere **49** (blue). The sulfone group in **49** induces less steric hindrance with ATM-specific Pro2775 (gray spheres) than the sulfone group in **27**.

suggested that *para*-H-bond acceptors were important and that an optimal interaction with the protein could be formed when the H-bond acceptor is positioned below the plane of the 6-phenyl ring. A set of *para*-amides (**32−38**) (Table 4) that have a range of in vacuo dihedral angles between the carbonyl and the plane of the 6-phenyl were used to assess this hypothesis. The piperidine amide **37**, with a natural dihedral angle of ∼60°, was the most potent in this series. This is consistent with the ATR homology model, which suggests that the dihedral angle in the co-complex is ∼65° for an optimal H-bond with Gly2385. For other amide analogues, the decreased potency can be explained by rotational energy barriers to the optimal ∼65° dihedral angle: for example, the primary amide **32**, which is conjugated with the phenyl ring, has to overcome a 6 kcal/mol barrier, which leads to a 4-fold reduction in potency (IC$_{50}$ of 110 nM as compared to an IC$_{50}$ of 26 nM for **37**). In the case of sulfone **27**, the improved potency is attributed to a low rotational energy barrier (<1 kcal/mol) to position a sulfone oxygen at the optimal angle and distance for a H-bond with the −NH− of Gly2385.

While the use of amides offers advantages in terms of the provision of chemical diversity, the requirement for favorable

dihedral angles for good H-bond interactions limits the possibilities. We therefore continued to explore the utility of sulfone **27**. Substituting the methyl-sulfone itself with both lipophilic (**40−44**) and polar groups (**45−47**) led to compounds with potency improvements of up to 4-fold, while retaining selectivity versus DNAPK and ATM. In addition, polar substitution (**45−47**) provided an enhancement in cell potency that may have been due to improved physical properties. Compound **45**, for example, has an enzyme potency of 12 nM and inhibits ATR-mediated phosphorylation of H2AX in cells with an IC$_{50}$ of 0.42 μM; in contrast, compound **42**, with a similar enzyme potency of 14 nM, inhibits ATR in cells with an IC$_{50}$ of 2 μM.

Besides its attractive combination of potency, selectivity, and cellular activity, compound **45** has good "druglike" properties that include aqueous solubility, lipophilicity (cLogP 3.0), and a

Table 4. Structures and Inhibitory Activities of Compounds 6, 27, and 32−47 against Selected Members of the PIKK Family

compd	R	enzyme inhibition IC$_{50}$ (μM)			cellular inhibition IC$_{50}$ (μM)
		ATR	ATM	DNAPK	ATR
6	−C$_6$H$_5$	0.62	>8	>8	>2.5
32	−C$_6$H$_4$-4-CONH$_2$	0.11	2.9	1.2	ND
33	−C$_6$H$_4$-4-CONHMe	0.18	2.6	7	ND
34	−C$_6$H$_4$-4-CO-azetidin-1-yl	0.10	>8	>8	1.0
35	−C$_6$H$_4$-4-CONMe$_2$	0.054	>8	>8	2.0
36	−C$_6$H$_4$-4-CO-pyrrolidin-1-yl	0.054	>8	2.8	1.4
37	−C$_6$H$_4$-4-CO-piperidin-1-yl	0.026	>8	>8	6.5
38	−C$_6$H$_4$-3-chloro-4-CONMe$_2$	0.048	>8	>8	12.0
39	-C$_6$H$_4$-4-SOMe	0.056	>8	6.8	5.4
27	−C$_6$H$_4$-4-SO$_2$Me	0.026	>8	4.4	0.8
40	−C$_6$H$_4$-4-SO$_2$Et	0.012	>8	5.8	1.5
41	−C$_6$H$_4$-4-SO$_2$iPr	0.008	>8	5.6	1.0
42	−C$_6$H$_4$-4-SO$_2$nPr	0.014	5.4	>8	2.0
43	−C$_6$H$_4$-4-SO$_2$sBu	0.010	6.6	>8	1.6
44	−C$_6$H$_4$-4-SO$_2$tBu	0.006	>8	>8	1.0
45	−C$_6$H$_4$-4-SO$_2$CH(Me)CH$_2$NMe$_2$	0.012	>8	>8	0.42
46	−C$_6$H$_4$-4-SO$_2$CH(Me)CH$_2$CH$_2$OH	0.008	>8	3.2	0.38
47	−C$_6$H$_4$-4-SO$_2$-(R)-THF	0.010	5	4.4	0.46

profile in Caco2 study that suggests good passive diffusion across membranes with minimal efflux liability (A−B = 17.10^{-6} cm/s, and B−A = 23.10^{-6} cm/s). It was therefore selected for further biological evaluation.

■ BIOLOGICAL EVALUATION OF SULFONE 45

Sulfone **45** is an ATP competitive inhibitor of ATR (Figure 5).[42] Secondary analysis, using the Morrison equation for tight binding, gives the inhibition constant K_i as 6 nM. Compound **45** displays excellent selectivity for ATR against the related PIKK family members ATM and DNAPK (IC$_{50}$ > 8 μM) and also against a panel of 50 unrelated kinases where in all cases the predicted IC$_{50}$ was >400 nM (data provided in the Supporting Information). Sulfone **45** blocks ATR activity in cells with an IC$_{50}$ of 0.42 μM, as determined by measurement of ATR-dependent phosphorylation of H2AX (Ser139) in hydroxyurea-treated HT29 cancer cells[37] (data shown in the Supporting Information). Because ATR has been shown to promote cell survival in response to naturally occurring DNA damage[43−45] or in response to DNA-damaging agents,[14,15,46−48] we looked at the effect of **45** both as a single agent and in combination with genotoxic agents in a representative cancer (HCT116) and normal (HFL1) cell lines. HCT116 cancer cells were selected for their known defects in the ATM signaling pathway[49,50] that is hypothesized to cause sensitivity to ATR inhibition. Sulfone **45** showed potent activity against these cancer cells (IC$_{50}$ of 1.1 μM), while in contrast it did not kill normal HFL1 cells, even at high concentrations (20 μM). The effect of **45** in combination with DNA-damaging agents was assessed with IR and the DNA cross-linking drug cisplatin. Data were analyzed using the MacSynergy software that represents synergistic and antagonistic

interactions as deviations above and below a plane that corresponds to additivity (Figure 6).[51] Marked synergy was observed for **45** in combination with both IR and cisplatin in the HCT116 cells across a range of IR intensity or cisplatin concentrations. In the case of cisplatin combinations, **45** at 0.62 μM was able to increase the potency of cisplatin by 7-fold. The effect was much reduced in the normal cell line (1.1-fold at 0.62 μM of **45**), and no synergy with IR was observed at all. The different responses to compound **45** in the normal and cancer cell lines support the hypothesis that cells lacking the ATM signaling pathway are reliant on ATR for survival following DNA damage.[27]

■ CONCLUSION

We have described the discovery of the first potent and highly selective inhibitors of ATR. This series of 3-amino-6-arylpyrazines inhibits ATR with an ATP competitive mechanism of action. The study of SARs and homology modeling has helped identify a number of interactions that are important for ATR potency and selectivity. Most importantly, an aromatic group at the 6-position of the pyrazine ring is required for optimal π-stack interactions with a tryptophan (Trp2379) in ATR. Appropriate substitution of this ring from the para-position enables an H-bond to be established with the backbone NH of an ATR-specific glycine residue (Gly2385) at the rim of the active site. The fact that ATR can tolerate a range of phenylamide isosteres at the 2-position of the pyrazine ring can be used to influence selectivity within the PIKK family. The most potent and selective compound from this series, sulfone **45**, inhibits ATR with a K_i of 6 nM, with excellent selectivity over the 50 or so kinases that we tested it against. These included the closely related PIKK family members ATM and DNA-PK (IC$_{50}$ > 8 μM).
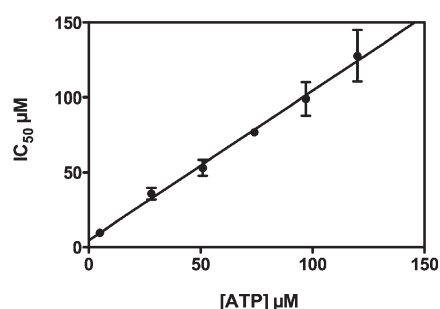
Figure 5. IC_{50} values for **45** against ATR were determined at different ATP concentrations [ranging from 0.5- to 12-fold K_m ($K_m = 10\,\mu M$)] in quadruplet. Mean IC_{50} values ($\pm$SEM) were plotted against ATP concentration and fit to the Cheng–Prussof equation for tight binding competitive inhibition [$IC_{50} = K_i(1 + [ATP]/K_m) + [E]/2$; $R^2 = 0.996$].

Consistent with the notion that cells with deficiencies in the complementary ATM-mediated DDR pathway may be reliant on ATR for survival following DNA damage, compound **45** showed potent cytotoxic activity against a cancer cell line with this defect. In contrast, it was not cytotoxic toward normal cells. The effect on ATM pathway-deficient cancer cells was magnified when DNA-damaging agents were used, and **45** markedly sensitized these cells to IR and the DNA cross-linking drug cisplatin. Sensitization was almost absent in the normal cells. These results provide more good evidence that an ATR inhibitor should provide a new means by which to enhance the efficacy of radiotherapy and well-established oncology drugs such as cisplatin.

The prospect of enhancing the efficacy of IR and other established genotoxic agents without enhancing collateral damages or side effects is potentially transformational in the treatment of cancer. In the context of tumors that have lost their ATM-p53 pathway function, a common lesion in cancer cells, an ATR inhibitor may be able to deliver such a desirable outcome. ATR inhibition therefore appears to provide a rare opportunity in cancer drug discovery where toxicity toward tumor cells can be enhanced in preference to normal tissue.

■ MATERIALS AND METHODS

General Experimental Section. All commercially available solvents and reagents were used as received. Microwave reactions were carried out using a CEM Discovery microwave. Analytical thin-layer chromatography was carried out using glass-backed plates coated with Merck Kieselgel 60 GF_{240}. Plates were visualized using UV light (254 or 366 nm) and/or by staining with potassium permanganate followed by heating. Flash chromatography was carried out on an ISCO Combiflash[R] Companion system eluting with a 0–100% EtOAc/petroleum ether gradient. Samples were applied preabsorbed on silica. Semipreparative reverse phase HPLC was carried out on a Waters autopurification HPLC-MS system equipped with a waters C-18 sunfire reverse phase column (19 mm × 150 mm, 5 μm). The mobile phases were acetonitrile (0.1% trifluoroacetic acid) and water (0.1% trifluoroacetic acid). ¹H NMR spectra were recorded at 400 MHz using a Bruker DPX 400 instrument. MS samples were analyzed on a MicroMass Quattro Micro mass spectrometer operated in single MS mode with electrospray ionization. Samples were introduced into the mass spectrometer using chromatography. All final products had a purity ≥95%, unless specified otherwise in the experimental details. The purity of the final compounds was determined using HPLC method: Analytical reverse phase HPLC-MS
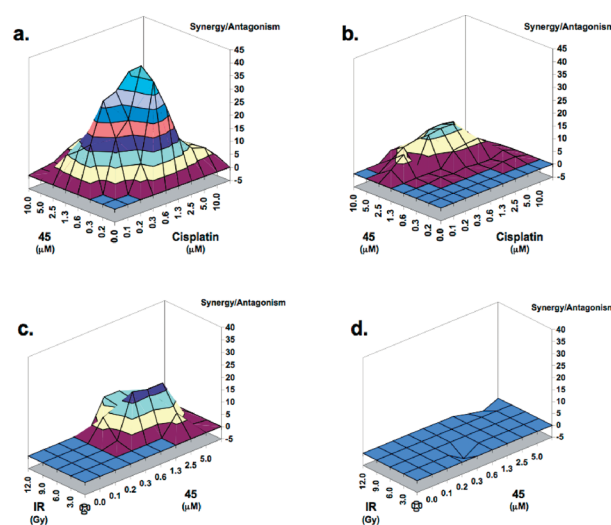

Figure 6. Macsynergy plots of **45** in combination with cisplatin in HCT116 cells (a), cisplatin in HFL1 cells (b), IR in HCT116 cells (c), and IR in HFL1 cells (d).

was carried out on an agilent 100 HPLC with a waters Quattro MS system equipped with an ACE 5 mm C-18 reverse phase column (4.6 mm × 150 mm, 5 μm). The mobile phases were acetonitrile/methanol (1:1) and water (10 mm ammonium acetate).

Method A: General Procedure for Suzuki Cross-Coupling; Compounds 6, 11–33, 35, and 39–41. To reaction tubes containing 3-amino-6-bromo-N-phenyl-pyrazine-2-carboxamide **8** (88 mg, 0.3 mmol) in DMF (4 mL) were added boronic acid or ester (0.3 mmol) followed by $Pd(PPh_3)_2Cl_2$ or $Pd(PPh_3)_4$ (5 mol %) and 2 M aqueous Na_2CO_3 solution (2 mL). The tubes were then flushed with N_2 and heated to 88 °C for 18 h. After this time, the reactions were allowed to cool to ambient temperature, filtered, and purified by reverse phase HPLC to give the desired products as solids after lyophilization (yields ranged from 10 to 90%). Analytical data for **6**, **11–33**, **35**, and **39–41** are provided in the Supporting Information.

Method B: General Procedure for Amide Derivatives; Compounds 34 and 36–38. To a solution of 4-[5-amino-6-(phenylcarbamoyl)pyrazin-2-yl]benzoic acid (preparation described in the Supporting Information) (50 mg, 0.15 mmol) in DMSO (1 mL) were sequentially added a required amine (0.45 mmol), CDI (49 mg, 0.3 mmol), DMAP (1.8 mg, 0.015 mmol), and DIPEA (78 μL, 0.45 mmol). The resulting solution was stirred at 40 °C for 6 h. The resulting solution was filtered and purified by reverse phase HPLC to the desired amide derivative (yields ranged from 35 to 74%). Analytical data for **34** and **36–38** are provided in the Supporting Information.

Method C: General Procedure for Sulfone Derivatives; Compounds 42–47. To a solution of a generic 1-bromo-4-(alkylsulfonyl)benzene (preparations described in the Supporting Information) (0.34 mmol) in dioxane (1 mL) was added bis-(pinacolato)diboron (130 mg, 0.5 mmol), followed by potassium acetate (100 mg, 1 mmol). The reaction was degassed with N_2 before $Pd(dppf)Cl_2 \cdot CH_2Cl_2$ (28 mg, 0.03 mmol) was added. The reaction was heated to 90 °C for 2 h, allowed to cool, and purged with N_2 for 10 min. 3-Amino-6-bromo-N-phenyl-pyrazine-2-carboxamide **8** (100 mg, 0.34 mmol) was then added, followed by an aqueous solution of Na_2CO_3 (512 μL of 2M, 1 mmol) and $Pd(PPh_3)_4$ (39 mg, 0.03 mmol). The reaction mixture was heated to 150 °C in a microwave reactor for 30 min, allowed to cool to room temperature, and filtered through an SCX-2 cartridge. The cartridge was washed with 200 mL of MeCN/MeOH, followed by 2 M NH_3 in MeOH with MeCN to elute the compound. Evaporation of the combined solvents gave a brown solid, which was

purified by reverse phase HPLC (yields ranged from 21 to 52%). Analytical data for **42**−**47** are provided in the Supporting Information.

3-Amino-*N*-phenylpyrazine-2-carboxamide (7). To a solution of 3-aminopyrazine-2-carboxylic acid **55** (100 mg, 0.72 mmol) in DME (2 mL) were added aniline (67 mg, 66 μL, 0.72 mmol), diethoxy-phosphorylformonitrile (130 mg, 119 μL, 0.72 mmol), and triethylamine (132 mg, 182 μL, 1.3 mmol). The reaction mixture was stirred at room temperature for 2 h and then partitioned between water and CH_2Cl_2 (3 × 50 mL). The combined organic layers were dried over $MgSO_4$ and concentrated to give an oil, which solidified upon standing. The solid was redissolved in MeCN and then purified by reverse phase HPLC to give 3-amino-*N*-phenylpyrazine-2-carboxamide **7** (66 mg, 44%) as a brown solid. MS (ES$^+$) *m/z* 215 (M + H)$^+$. ^{1}H NMR (400 MHz, DMSO-d_6): δ 10.51 (s, 1H), 8.29 (d, 1H), 7.93 (d, 1H), 7.85−7.82 (m, 2H), 7.62 (s, 2H), 7.36 (dd, 2H) and 7.12 (dd, 1H) ppm. ^{13}C NMR (100 MHz, DMSO-d_6): δ 164.91, 155.82, 147.71, 138.51, 131.31, 128.99, 125.73, 124.26, 120.79 ppm. HRMS (ES$^+$) calcd for $C_{11}H_{11}N_4O$ (M + H)$^+$, 215.0933; found, 215.0943.

3-Amino-6-bromo-*N*-phenylpyrazine-2-carboxamide (8). To a solution of 3-amino-6-bromo-pyrazine-2-carboxylic acid **56** (10 g, 46 mmol) in DMSO (100 mL) were added CDI (15 g, 92 mmol), DIPEA (6.5 g, 8.8 mL, 50 mmol), and DMAP (280 mg, 2.3 mmol). The reaction mixture was stirred for 30 min, and then, aniline (4.3 g, 4.2 mL, 46 mmol) was added, and the resulting solution was stirred at room temperature for 18 h. Water was then added, and the product was collected by filtration to give 3-amino-6-bromo-*N*-phenyl-pyrazine-2-carboxamide **8** (13 g, 92%) as a brown powder. MS (ES$^+$) *m/z* 294 (M + H)$^+$. ^{1}H NMR (400 MHz, DMSO-d_6): δ 10.22 (s, 1H), 8.36 (d, 1H), 7.73−7.71 (m, 2H), 7.68 (s, 2H), 7.29 (dd, 2H), and 7.06 (t, 1H) ppm. HRMS (ES$^+$) calcd for $C_{11}H_{10}BrN_4O$, 293.0038; found, 293.0049.

3-Amino-6-cyclohexyl-*N*-phenylpyrazine-2-carboxamide (9). A solution of 3-amino-6-(cyclohex-1-en-1-yl)-*N*-phenylpyrazine-2-carboxamide **10** (30 mg) in EtOH (5 mL) was passed though an H-cube fitted with a Pd/C catalyst cartridge with a flow rate of 0.5 mL/min at 35 °C. The solvent was removed in vacuo, and the resulting pale yellow solid was purified by reverse phase HPLC to yield 3-amino-6-cyclohexyl-*N*-phenylpyrazine-2-carboxamide **9** (11 mg, 36%) as a yellow solid. MS (ES$^+$) *m/z* 297 (M + H)$^+$. ^{1}H NMR (400 MHz, DMSO-d_6): δ 10.19 (s, 1H), 8.24 (s, 1H), 7.78 (d, 2H), 7.41 (br s, 2H), 7.40−7.36 (m, 2H), 7.14 (t, 1H), 2.73−2.65 (m, 1H), 1.88 (d, 2H), 1.82 (d, 2H), 1.72 (d, 1H), 1.59 (td, 2H) and 1.43−1.24 (m, 3H) ppm. HRMS (ES$^+$) calcd for $C_{17}H_{21}N_4O$, 297.1715; found, 297.1723.

3-Amino-6-(cyclohex-1-en-1-yl)-*N*-phenylpyrazine-2-carboxamide (10). To a solution of 3-amino-6-bromo-*N*-phenylpyrazine-2-carboxamide **8** (300 mg, 1 mmol) and 2-(1-cyclohexenyl)-4,4,5,5-tetramethyl-1,3,2-dioxaborolane (330 μL, 1.5 mmol) in DMF (3 mL) were added Pd(PPh$_3$)$_4$ (118 mg, 0.1 mmol) and a 2 M aqueous solution of Na$_2$CO$_3$ (1.5 mL, 3 mmol). The resulting solution was stirred at 90 °C for 3 h. The solution was then allowed to cool, water was added, and the mixture was extracted with CH_2Cl_2 (3 × 10 mL). The combined organic layers were concentrated, and the residue was purified by reverse phase HPLC to give 3-amino-6-(1-cyclohexenyl)-*N*-phenyl-pyrazine-2-carboxamide **10** (134 mg, 40%) as an orange solid. MS (ES$^+$) *m/z* 295 (M + H)$^+$. ^{1}H NMR (400 MHz, DMSO-d_6): δ 10.18 (s, 1H), 8.50 (d, 1H), 7.78 (d, 2H), 7.50 (s, 2H), 7.41−7.36 (m, 2H), 7.14 (t, 1H), 6.71 (t, 1H), 2.23 (d, 2H), and 1.78−1.62 (m, 6H) ppm. ^{13}C NMR (101.0 MHz, DMSO): δ 164.95, 154.08, 143.93, 141.08, 138.22, 133.49, 129.04, 126.04, 124.41, 123.06, 120.97, 25.61, 25.06, 22.68, and 22.11 ppm. HRMS (ES$^+$) calcd for $C_{17}H_{19}N_4O$ (M + H)$^+$, 295.1559; found, 295.1558. Purity, 89% (method 2).

3-Amino-6-(4-((1-(dimethylamino)propan-2-yl)sulfonyl)-phenyl)-*N*-phenylpyrazine-2-carboxamide (45). Prepared from 2-(4-bromophenyl)sulfonyl-*N*,*N*-dimethyl-propan-1-amine (see the Supporting Information) according to method C; yellow solid. MS (ES$^+$)

m/z 440 (M + H)$^+$. ^{1}H NMR (400 MHz, DMSO-d_6): δ 10.47 (s, 1H), 9.08 (d, 1H), 8.60 (d, 2H), 8.00 (d, 2H), 7.94 (s, 2H), 7.82 (d, 2H), 7.42 (t, 2H), 7.18 (t, 1H), 4.09 (s, 1H), 3.34 (d, 1H), 2.83 (s, 3H), 2.80 (s, 3H), 2.55 (t, 1H), and 1.29 (d, 3H) ppm. ^{13}C NMR (101.0 MHz, DMSO-d_6): δ 164.73, 155.14, 145.79, 141.06, 138.20, 137.06, 136.69, 129.21, 128.99, 126.41, 124.87, 124.68, 121.64, 58.77, 57.26, 45.59, and 12.40 ppm. HRMS (ES$^+$) calcd for $C_{22}H_{26}N_5O_3S$ (M + H)$^+$, 440.1756; found, 440.1741.

3-Amino-*N*-cyclohexyl-6-(4-(methylsulfonyl)phenyl)pyrazine-2-carboxamide (48). To a suspension of methyl 3-amino-6-bromo-pyrazine-2-carboxylate **54** (10 g, 43.1 mmol) in DME (125 mL) at room temperature were added (4-methylsulfonylphenyl)boronic acid (10.35 g, 51.7 mmol) followed by PdCl$_2$(PPh$_3$)$_2$ (1.51 g, 2.15 mmol) and Na$_2$CO$_3$ (64.6 mL of 2 M, 129.3 mmol). The reaction mixture was heated at 90 °C for 9 h. After it was cooled to room temperature, the solid was collected by filtration, washed with DME, and dissolved into water. The aqueous solution was acidified to pH 1 with 1 M HCl. The precipitate was collected by filtration and dried under vacuum to give 3-amino-6-(4-methylsulfonylphenyl)pyrazine-2-carboxylic acid **57** as a yellow solid (11.5 g, 91%). ^{1}H NMR (400 MHz, DMSO-d_6): δ 13.20 (br s, 1H), 9.03 (s, 1H), 8.35 (d, 2H), 8.00 (d, 2H), 7.70 (br s, 2H), and 3.25 (s, 3H) ppm. ^{13}C NMR (101.0 MHz, DMSO-d_6): δ 167.95, 155.70, 146.08, 141.08, 140.19, 137.52, 127.82, 126.21, 123.15, 43.95 ppm. MS (ES$^+$) *m/z* 294 (M + H)$^+$.

To a solution of 3-amino-6-(4-methylsulfonylphenyl)pyrazine-2-carboxylic acid **57** (100 mg, 0.34 mmol) in DME (1 mL) were added cyclohexylamine (51 mg, 59 μL, 0.51 mmol), diethoxy-phosphorylformonitrile (111 mg, 0.68 mmol), and DIPEA (132 mg, 178 μL, 1.02 mmol). The reaction mixture was heated at 100 °C for 10 min under microwave conditions. The reaction mixture was then filtered and purified by reverse phase HPLC to give the title product as a yellow solid (88 mg, 69%). MS (ES$^+$) *m/z* 375 (M + H)$^+$. ^{1}H NMR (400 MHz, DMSO-d_6): δ 8.95 (s, 1H), 8.47 (d, 1H), 8.40 (d, 2H), 7.99 (d, 2H), 3.82 (d, 1H), 3.26 (s, 3H), 1.84−1.74 (m, 4H), 1.64 (d, 1H), 1.50 (dd, 2H), 1.34 (d, 2H), and 1.19 (s, 1H) ppm. ^{13}C NMR (101.0 MHz, DMSO): δ 165.06, 159.94, 145.06, 141.15, 140.11, 136.59, 127.72, 126.40, 125.25, 48.30, 43.96, 32.44, 25.55, and 25.28 ppm. HRMS (ES$^+$) calcd for $C_{18}H_{23}N_4O_3S$ (M + H)$^+$, 375.1491; found, 375.1491.

3-(1*H*-Benzo[*d*]imidazol-2-yl)-5-(4-(methylsulfonyl)phenyl)-pyrazin-2-amine (49). To a solution of 3-amino-6-bromo-pyrazine-2-carboxylic acid **56** (900 mg, 4.1 mmol) in DME (27 mL) were added phenylenediamine (491 mg, 4.5 mmol), diethoxyphosphorylformonitrile (741 mg, 673 μL, 4.5 mmol), and triethylamine (835 mg, 1.2 mL, 8.3 mmol). The reaction mixture was heated in the microwave at 170 °C for 20 min and cooled to room temperature before water was added. The formed precipitate was collected and washed with a small amount of ether to give 3-(1*H*-benzo[*d*]imidazol-2-yl)-5-bromopyrazin-2-amine **58** (553 mg, 43%) as a yellow solid. MS (ES$^+$) *m/z* 291 (M + H)$^+$. ^{1}H NMR (400 MHz, DMSO-d_6): δ 13.09 (s, 1H), 8.29 (s, 1H), 7.76 (d, 1H), 7.58 (d, 1H), and 7.33−7.24 (m, 2H) ppm.

To a solution of 3-(1*H*-benzimidazol-2-yl)-5-bromo-pyrazin-2-amine **58** (100 mg, 0.3 mmol) in DME (1.25 mL) were added (4-methylsulfonylphenyl)boronic acid (69 mg, 0.3 mmol) followed by Pd(PPh$_3$)$_2$Cl$_2$ (12 mg, 0.02 mmol) and a 2 M aqueous solution of sodium carbonate (517 μL, 1 mmol). The reaction mixture was heated in microwave for 3 h at 150 °C, cooled to room temperature, diluted with EtOAc (50 mL), washed with water (50 mL), and extracted with EtOAc (3 × 50 mL). The combined organic layers were dried (MgSO$_4$) and concentrated. The residue was purified by reverse phase HPLC to give 3-(1*H*-benzo-[*d*]imidazol-2-yl)-5-(4-(methylsulfonyl)-phenyl)pyrazin-2-amine **49** as a yellow solid (53 mg, 48%). MS (ES$^+$) *m/z* 366 (M + H)$^+$. ^{1}H NMR (400 MHz, DMSO-d_6): δ 13.2 (s, 1H), 8.95 (s, 2H), 8.58 (d, 2H), 8.05 (d, 2H), 7.8 (d, 1H), 7.67 (d, 1H), 7.2−7.38 (m, 2H), 3.4 (s, 3H) ppm. ^{13}C NMR (101.0 MHz, DMSO): δ 153.44, 150.50, 143.31, 142.30, 141.56, 140.03, 137.12, 134.41, 127.71, 126.11, 125.41, 124.21, 122.54,

Table 5. Parameters for Kinase Activity Assays

assay	[kinase] (nM)[d]	target peptide[e]	[peptide] (mM)[d]	[ATP] (mM)[d]	μCi [γ-^{33}P] ATP per nmol ATP	time course (h)[f]
ATR[a]	5	ASELPASQPQPFSAKKK	0.8	0.01	0.8	24
ATM[b]	50	DPSVEPPLSQETFSDKKK	0.02	0.02	2.1	24
DNAPK[c]	4	EPPLSQEAFADLWKKK	0.8	0.11	0.3	2

[a] Assay buffer: 50 mM Tris-HCl (pH 7.5), 10 mM MgCl$_2$, and 1 mM DTT. [b] Assay buffer: 10 mM HEPES (pH 7.5), 5 mM MgCl$_2$, 5 mM MnCl$_2$, 100 mM NaCl, 0.1% BSA, and 1 mM DTT. [c] Assay buffer: 50 mM HEPES (pH 7.5), 10 mM MgCl$_2$, 100 mM KCl, 0.2 mM EGTA, 0.1 mM EDTA, 0.01% BSA, 5 μg/mL calf thymus DNA, and 1 mM DTT. [d] Final assay concentration. [e] Primary amino acid sequence. [f] The duration of the enzyme assay was guided by the activity of the enzyme; for both ATR and ATM, low enzyme activity necessitated an extended assay to ensure sufficient activity for detection. In all cases (data not reported), previous studies had been run to ensure linearity of the reaction progress curves throughout the duration of the enzyme assay.

119.60, 112.21, and 43.99 ppm. HRMS (ES$^+$) calcd for C$_{18}$H$_{16}$N$_5$O$_2$S (M + H)$^+$, 366.1025; found, 366.1042. Purity, 90% (method 1).

3-(Benzoxazol-2-yl)-5-(4-(methylsulfonyl)phenyl)pyrazin-2-amine (50). To a solution of 3-amino-6-bromo-pyrazine-2-carbonitrile **59** (500 mg, 2.5 mmol) in DME (2.5 mL) was added 2-aminophenol (109.7 mg, 2.5 mmol). The reaction mixture was stirred at 150 °C in the microwave for 60 min, cooled to room temperature, and filtered. The solid was washed with diethyl ether to give 3-(1,3-benzoxazol-2-yl)-5-bromo-pyrazin-2-amine **60** (353 mg, 48%) as a sandy solid. MS (ES$^+$) m/z 291 (M + H)$^+$. ^{1}H NMR (400 MHz, DMSO-d_6): δ 8.44 (s, 1H), 8.09 (s, 2H), 7.91−7.89 (m, 2H), and 7.51 (m, 2H) ppm.

To a solution of 3-(1,3-benzoxazol-2-yl)-5-bromo-pyrazin-2-amine **60** (68 mg, 0.2 mmol) in dioxane (1 mL) were added (4-methylsulfonylphenyl)boronic acid (47 mg, 0.2 mmol) and a 2 M aqueous solution of Na$_2$CO$_3$ (234 μL, 0.47 mmol). The resulting suspension was purged with N$_2$, and Pd(PPh$_3$)$_4$ (27 mg, 0.02 mmol) was added. The reaction mixture was heated in the microwave at 110 °C for 30 min, cooled to room temperature, and diluted with water. The solid was collected by filtration, washed with a water, dried, and then redissolved in DMSO; the resulting solution was purified by reverse phase HPLC to give 3-(1,3-benzoxazol-2-yl)-5-(4-methylsulfonylphenyl)pyrazin-2-amine **50** as a yellow solid (45 mg, 61%). MS (ES$^+$) m/z 295 (M + H)$^+$. ^{1}H NMR (400 MHz, DMSO-d_6): δ 9.05 (s, 1H), 8.37 (d, 2H), 8.24 (s, 2H), 8.07 (d, 2H), 7.96−7.93 (m, 2H), 7.56−7.48 (m, 2H), and 3.34 (s, 3H) ppm. ^{13}C NMR (101.0 MHz, DMSO-d_6): δ 160.78, 153.96, 149.99, 144.26, 140.84, 140.34, 138.29, 128.00, 126.84, 126.21, 125.64, 121.97, 120.44, 111.65, 43.99 ppm. HRMS (ES$^+$) calcd for C$_{18}$H$_{15}$N$_4$O$_3$S (M + H)$^+$, 367.0865; found, 367.0865.

3-(Benzo[d]thiazol-2-yl)-5-(4-(methylsulfonyl)phenyl)-pyrazin-2-amine (51). This compound was prepared from 2-aminobenzenethiol according to the procedure used for **50**; yellow solid (29 mg, 38%). MS (ES$^+$) m/z 383 (M + H)$^+$. ^{1}H NMR (400 MHz, DMSO-d_6): δ 8.89 (s, 1H), 8.42 (d, 2H), 8.26 (d, 2H), 8.26 (d, 1H), 8.17 (d, 1H), 7.75−7.64 (m, 2H), and 3.31 (s, 3H) ppm. ^{13}C NMR (101.0 MHz, DMSO): δ 169.49, 153.62, 152.38, 144.11, 141.01, 140.35, 137.78, 134.73, 128.05, 127.33, 127.07, 126.52, 125.98, 123.55, 122.71, and 43.98 ppm. HRMS (ES$^+$) calcd for C$_{18}$H$_{15}$N$_4$O$_2$S$_2$ (M + H)$^+$, 383.0636; found, 383.0640.

3-(1H-Indol-2-yl)-5-(4-(methylsulfonyl)phenyl)pyrazin-2-amine (52). To a solution of 3,5-dibromopyrazin-2-amine **62** (100 mg, 0.4 mmol) in DME (1 mL) were added tert-butyl 2-(4,4,5,5-tetramethyl-1,3,2-dioxaborolan-2-yl)indole-1-carboxylate (130 mg, 0.4 mmol) followed by a 2 M aqueous solution of NaHCO$_3$ (0.6 mL, 1.2 mmol) and Pd(PPh$_3$)$_4$ (22 mg, 0.02 mmol). The reaction mixture was heated at 120 °C in the microwave for 10 min, allowed to cool to room temperature, and then purged with N$_2$. (4-Methylsulfonylphenyl)-boronic acid (80 mg, 0.4 mmol) was added, and the reaction was heated at 120 °C in the microwave for a further 10 min. The mixture was partitioned between ethyl acetate, extracted with EtOAc (2 × 5 mL), dried (MgSO$_4$), and concentrated in vacuo. The residue was dissolved in a mixture TFA/CH$_2$Cl$_2$ (1/1, 15 mL), and the reaction was stirred overnight at room

temperature. The mixture was neutralized with aqueous Na$_2$CO$_3$ (50 mL) and extracted with CH$_2$Cl$_2$ (2 × 50 mL). The combined organic layers were concentrated in vacuo, and the residue was purified by reverse phase HPLC to give 3-(1H-indol-2-yl)-5-(4-methylsulfonyl phenyl)pyrazin-2-amine **52** as a yellow solid (39 mg, 27%). MS (ES$^+$) m/z 365 (M + H)$^+$. ^{1}H NMR (400 MHz, DMSO-d_6): δ 11.58 (s, 1H), 8.75 (s, 1H), 8.53 (d, 2H), 8.01 (d, 2H), 7.63 (d, 1H), 7.58 (d, 1H), 7.30 (d, 1H), 7.21 (t, 1H), 7.06 (t, 1H), 6.85 (s, 2H), and 3.28 (s, 3H) ppm. ^{13}C NMR (100 MHz, DMSO-d_6): δ 152.26, 141.96, 139.86, 138.78, 137.56, 137.10, 133.72, 130.82, 128.86, 127.66, 126.21, 123.28, 121.26, 119.82, 112.09, 102.95 ppm. HRMS (ES$^+$) calcd for C$_{19}$H$_{17}$N$_4$O$_2$S (M + H)$^+$, 365.1072; found, 365.1066.

Kinase Inhibition Assays. *Materials and Reagents.* HEPES, Tris-HCl, NaCl, KCl, MnCl$_2$, MgCl$_2$, EGTA, EDTA, BSA, ATP, phosphoric acid, calf thymus DNA, and DMSO were supplied by Sigma-Aldrich. DTT was from Melford Laboratories. Target peptides were synthesized at Biomol International LP. Stock 3 mCi/mmol [γ-^{33}P]ATP and Optiphase Supermix scintillation cocktail were supplied by Perkin-Elmer. Phosphocellulose capture plates (MSPHNXB) were from Millipore. Full-length ATR and ATM kinases were produced in-house using methods based on published protocols,[52] and DNAPK was purchased from Promega.

Kinase Inhibition Assays. The ability of compounds to inhibit ATR, ATM or DNAPK kinase activity was tested using a radiometric-phosphate incorporation assay,[53] as described in Table 5 and below. A stock solution was prepared consisting of the appropriate buffer, kinase, and target peptide. To this was added the compound of interest, at varying concentrations in DMSO to a final DMSO concentration of 7%. Assays were initiated by addition of an appropriate [g-^{33}P]ATP solution and incubated at 25 °C. Assays were stopped, after the desired time course, by addition of phosphoric acid and ATP to a final concentration of 100 mM and 0.66 μM, respectively. Peptides were captured on a phosphocellulose membrane, prepared as per manufacturer's instructions, and washed six times with 200 μL of 100 mM phosphoric acid, prior to the addition of 100 μL of scintillation cocktail and scintillation counting on a 1450 Microbeta Liquid Scintillation Counter (Perkin-Elmer). Dose−response data were analyzed using GraphPad Prism software (Version 3.0cx for Macintosh, GraphPad Software).

Cellular Assays. Cell lines were purchased from ATCC and maintained according to the distributor's instructions. Cell assays were performed using exponentially growing cultures. For H2AX phosphorylation analysis using immunofluorescence (IF) microscopy, cells were fixed in 4% formaldehyde, permeabilized with 0.5% Triton X-100, and stained with mouse H2AX pS139 antibody (Upstate), AlexaFluor 488 goat antimouse antibody (Invitrogen), and Hoechst (Invitrogen). The cells were then analyzed using the BD Pathway 855 bioimager and BD Attovision software. The cell density was analyzed using the CellTiter 96 AQueous Cell Proliferation (MTS) assay (Promega). Cells were plated in 96-well plates and allowed to adhere overnight. The following day, compounds were added at the indicated concentrations in a final volume of 200 μL, and the cells were then incubated for 96 h. MTS reagent

(40 μL) was then added, and 1 h later, absorbance at 490 nm was measured using a SpectraMax Plus 384 plate reader (Molecular Devices). Synergy and antagonism were assessed using Macsynergy software.[51]

■ ASSOCIATED CONTENT

ⓢ Supporting Information. Formulas, experimental procedures, and analytical data for key intermediates and for compounds not specifically described in the main text; a summary of biological evaluation for **6**−**52**; and the full selectivity profile of **45**. This material is available free of charge via the Internet at http://pubs.acs.org.

■ AUTHOR INFORMATION

Corresponding Author
*Tel: +44(0)1235 438800. Fax: +44(0)1235 820440. E-mail: john_pollard@vrtx.com.

■ ACKNOWLEDGMENT

■ ABBREVIATIONS USED

ATM, ataxia telangiectasia mutated; ATP, adenosine-5′-triphosphate; ATR, ataxia telangiectasia mutated and Rad3 related; DNA-PK, DNA-dependent protein kinase; DDR, DNA damage response; HTS, high-throughput screen; IR, ionizing radiation; PIKK, phosphoinositol 3-kinase-like kinase; PARP, poly-ADP-ribose polymerase; PI3K-γ, phosphatidylinositol 3-kinase γ; SAR, structure−activity relationship

■ REFERENCES

(1) Einhorn, L. H. Curing metastatic testicular cancer. *Proc. Natl. Acad. Sci. U.S.A.* **2002**, *99*, 4592–4595.

(2) Longley, D. B.; Johnston, P. G. Molecular mechanisms of drug resistance. *J. Pathol.* **2005**, *205*, 275–292.

(3) Borst, P.; Rottenberg, S.; Jonkers, J. How do real tumors become resistant to cisplatin?. *Cell Cycle* **2008**, *7*, 1353–1359.

(4) Oliver, T. G.; Mercer, K. L.; Sayles, L. C.; Burke, J. R.; Mendus, D.; Lovejoy, K. S.; Cheng, M.-H.; Subramanian, A.; Mu, D.; Powers, S.; Crowley, D.; Bronson, R. T.; Whittaker, C. A.; Bhutkar, A.; Lippard, S. J.; Golub, T.; Thomale, J.; Jacks, T.; Sweet-Cordero, E. A. Chronic cisplatin treatment promotes enhanced damage repair and tumor progression in a mouse model of lung cancer. *Genes Dev.* **2010**, *24*, 837–852.

(5) Olaussen, K. A.; Dunant, A.; Fouret, P.; Brambilla, E.; André, F.; Haddad, V.; Taranchon, E.; Filipits, M.; Pirker, R.; Popper, H. H.; Stahel, R.; D., M.; Sabatier, L.; Pignon, J.-P.; Tursz, T.; Le Chevalier, T.; Soria, J.-C. DNA repair by ERCC1 in non-small-cell lung cancer and cisplatin-based adjuvant chemotherapy. *N. Engl. J. Med.* **2006**, *355*, 983–991.

(6) Jackson, S. P.; Bartek, J. The DNA-damage response in human biology and disease. *Nature* **2009**, *461*, 1071–1078.

(7) Kastan, M. B.; Bartek, J. Cell-cycle checkpoints and cancer. *Nature* **2004**, *432*, 316–323.

(8) Cimprich, K. A.; Cortez, D. ATR: An essential regulator of genome integrity. *Nat. Rev. Mol. Cell Biol.* **2008**, *9*, 616–627.

(9) Jiang, H.; Reinhardt, H. C.; Bartkova, J.; Tommiska, J.; Blomqvist, C.; Nevanlinna, H.; Bartek, J.; Yaffe, M. B.; Hemann, M. T. The combined status of ATM and p53 link tumor development with therapeutic response. *Genes Dev.* **2009**, *23*, 1895–1909.

(10) Ding, L.; Getz, G.; Wheeler, D. A.; Mardis, E. R.; McLellan, M. D.; Cibulskis, K.; Sougnez, C.; Greulich, H.; Muzny, D. M.; Morgan, M. B.; Fulton, L.; Fulton, R. S.; Zhang, Q.; Wendl, M. C.; Lawrence, M. S.; Larson, D. E.; Chen, K.; Dooling, D. J.; Sabo, A.; Hawes, A. C.; Shen, H.; Jhangiani, S. N.; Lewis, L. R.; Hall, O.; Zhu, Y.; Mathew, T.; Ren, Y.; Yao, J.; Scherer, S. E.; Clerc, K.; Metcalf, G. A.; Ng, B.; Milosavljevic, A.; Gonzalez-Garay, M. L.; Osborne, J. R.; Meyer, R.; Shi, X.; Tang, Y.; Koboldt, D. C.; Lin, L.; Abbott, R.; Miner, T. L.; Pohl, C.; Fewell, G.; Haipek, C.; Schmidt, H.; Dunford-Shore, B. H.; Kraja, A.; Crosby, S. D.; Sawyer, C. S.; Vickery, T.; Sander, S.; Robinson, J.; Winckler, W.; Baldwin, J.; Chirieac, L. R.; Dutt, A.; Fennell, T.; Hanna, M.; Johnson, B. E.; Onofrio, R. C.; Thomas, R. K.; Tonon, G.; Weir, B. A.; Zhao, X.; Ziaugra, L.; Zody, M. C.; Giordano, T.; Orringer, M. B.; Roth, J. A.; Spitz, M. R.; Wistuba, I. I.; Ozenberger, B.; Good, P. J.; Chang, A. C.; Beer, D. G.; Watson, M. A.; Ladanyi, M.; Broderick, S.; Yoshizawa, A.; Travis, W. D.; Pao, W.; Province, M. A.; Weinstock, G. M.; Varmus, H. E.; Gabriel, S. B.; Lander, E. S.; Gibbs, R. A.; Meyerson, M.; Wilson, R. K. Somatic mutations affect key pathways in lung adenocarcinoma. *Nature* **2008**, *455*, 1069–1075.

(11) Bolt, J.; Vo, Q. N.; Kim, W. J.; McWhorter, A. J.; Thomson, J.; Hagensee, M. E.; Friedlander, P.; Brown, K. D.; Gilbert, J. The ATM/ p53 pathway is commonly targeted for inactivation in squamous cell carcinoma of the head and neck (SCCHN) by multiple molecular mechanisms. *Oral Oncol.* **2005**, *41*, 1013–1020.

(12) Greenman, C.; Stephens, P.; Smith, R.; Dalgliesh, G. L.; Hunter, C.; Bignell, G.; Davies, H.; Teague, J.; Butler, A.; Stevens, C.; Edkins, S.; O'Meara, S.; Vastrik, I.; Schmidt, E. E.; Avis, T.; Barthorpe, S.; Bhamra, G.; Buck, G.; Choudhury, B.; Clements, J.; Cole, J.; Dicks, E.; Forbes, S.; Gray, K.; Halliday, K.; Harrison, R.; Hills, K.; Hinton, J.; Jenkinson, A.; Jones, D.; Menzies, A.; Mironenko, T.; Perry, J.; Raine, K.; Richardson, D.; Shepherd, R.; Small, A.; Tofts, C.; Varian, J.; Webb, T.; West, S.; Widaa, S.; Yates, A.; Cahill, D. P.; Louis, D. N.; Goldstraw, P.; Nicholson, A. G.; Brasseur, F.; Looijenga, L.; Weber, B. L.; Chiew, Y. E.; DeFazio, A.; Greaves, M. F.; Green, A. R.; Campbell, P.; Birney, E.; Easton, D. F.; Chenevix-Trench, G.; Tan, M. H.; Khoo, S. K.; Teh, B. T.; Yuen, S. T.; Leung, S. Y.; Wooster, R.; Futreal, P. A.; Stratton, M. R. Patterns of somatic mutation in human cancer genomes. *Nature* **2007**, *446*, 153–158.

(13) Halazonetis, T. D.; Gorgoulis, V. G.; Bartek, J. An oncogene-induced DNA damage model for cancer development. *Science* **2008**, *319*, 1352–1355.

(14) Nghiem, P.; Park, P. K.; Kim, Y.; Vaziri, C.; Schreiber, S. L. ATR inhibition selectively sensitizes G1 checkpoint-deficient cells to lethal premature chromatin condensation. *Proc. Natl. Acad. Sci. U.S.A.* **2001**, *98*, 9092–9097.

(15) Nghiem, P.; Park, P. K.; Kim, Y. Y.; Desai, B. N.; Schreiber, S. L. ATR is not required for p53 activation but synergizes with p53 in the replication checkpoint. *J. Biol. Chem.* **2002**, *277*, 4428–4434.

(16) Reinhardt, H. C.; Jiang, H.; Hemann, M. T.; Yaffe, M. B. Exploiting synthetic lethal interactions for targeted cancer therapy. *Cell Cycle* **2009**, *8*, 3112–3119.

(17) Audeh, M. W.; Carmichael, J.; Penson, R. T.; Friedlander, M.; Powell, B.; Bell-McGuinn, K. M.; Scott, C.; Weitzel, J. N.; Oaknin, A.; Loman, N.; Lu, K.; Schmutzler, R. K.; Matulonis, U.; Wickens, M.; Tutt, A. Oral poly(ADP-ribose) polymerase inhibitor olaparib in patients with BRCA1 or BRCA2 mutations and recurrent ovarian cancer: a proof-of-concept trial. *Lancet* **2010**, *376*, 245–251.

(18) Tutt, A.; Robson, M.; Garber, J. E.; Domchek, S. M.; Audeh, M. W.; Weitzel, J. N.; Friedlander, M.; Arun, B.; Loman, N.; Schmutzler, R. K.; Wardley, A.; Mitchell, G.; Earl, H.; Wickens, M.; Carmichael, J. Oral poly(ADP-ribose) polymerase inhibitor olaparib in patients with BRCA1 or BRCA2 mutations and advanced breast cancer: A proof-of-concept trial. *Lancet* **2010**, *376*, 235–244.

(19) Hickson, I.; Zhao, Y.; Richardson, C. J.; Green, S. J.; Martin, N. M. B.; Orr, A. I.; Reaper, P. M.; Jackson, S. P.; Curtin, N. J.; Smith, G. C. M. Identification and Characterization of a Novel and Specific Inhibitor of the Ataxia-Telangiectasia Mutated Kinase ATM. *Cancer Res.* **2004**, *64*, 9152–9159.

(20) Griffin, R. J.; Fontana, G.; Golding, B. T.; Guiard, S.; Hard-castle, I. R.; Leahy, J. J. J.; Martin, N.; Richardson, C.; Rigoreau, L.; Stockley, M.; Smith, G. C. M. Selective Benzopyranone and Pyrimido[2,1-a]isoquinolin-4-one Inhibitors of DNA-Dependent Protein Kinase: Synthesis, Structure-Activity Studies, and Radiosensitization of a Human Tumor Cell Line in Vitro. *J. Med. Chem.* **2005**, *48* (2), 569–585.

(21) Zabludoff, S. D.; Deng, C.; Grondine, M. R.; Sheehy, A. M.; Ashwell, S.; Caleb, B. L.; Green, S.; Haye, H. R.; Horn, C. L.; Janetka, J. W.; Liu, D.; Mouchet, E.; Ready, S.; Rosenthal, J. L.; Queva, C.; Schwartz, G. K.; Taylor, K. J.; Tse, A. N.; Walker, G. E.; White, A. M. AZD a novel checkpoint kinase inhibitor, drives checkpoint abrogation and potentiates DNA-targeted therapies. *Mol. Cancer Ther.* **2008**, *7* (9), 2955–2966.

(22) Sarkaria, J. N.; Busby, E. C.; Tibbetts, R. S.; Roos, P.; Taya, Y.; Karnitz, L. M.; Abraham, R. T. Inhibition of ATM and ATR kinase activities by the radiosensitizing agent, caffeine. *Cancer Res.* **1999**, *59*, 4375–4382.

(23) Nishida, H.; Tatewaki, N.; Nakajima, Y.; Magara, T.; Ko, K. M.; Hamamori, Y.; Konishi, T. Inhibition of ATR protein kinase activity by schisandrin B in DNA damage response. *Nucleic Acids Res.* **2009**, *37*, 5678–5689.

(24) Wagner, J. M.; Kaufmann, S. H. Prospects for the Use of ATR Inhibitors to Treat Cancer. *Pharmaceuticals* **2010**, *3*, 1311–1334.

(25) Charrier, J.-D.; Durrant, S.; Kay, D.; O'Donnell, M.; Knegtel, R.; Maccormick, S.; Pinder, J.; Virani, A.; Young, S.; Binch, H.; Cleveland, T.; Fanning, L. T. D.; Hurley, D.; Joshi, P.; Sheth, U.; Silina, A. Preparation of pyrazine compounds as inhibitors of ATR kinase for use in treating disease and as biological tools; WO 2010054398.

(26) Charrier, J.-D.; Durrant, S.; Kay, D.; Knegtel, R.; MacCormick, S.; Mortimore, M.; O'Donnell, M.; Pinder, J.; Rutherford, A.; Virani, A. N.; Young, S.; Reaper, P. M. Pyrazine derivatives useful as inhibitors of ATR kinase and their preparation and use in the treatment of diseases; WO 2010071837.

(27) Foote, K. M.; Nissink, J.; Wilhelmus, M. Pyrimidinyl indole derivatives, and their preparation and use for prevention or treatment of tumors which are sensitive to inhibition of ATR kinase cancer; WO 2010073034.

(28) Ellingson, R. C.; Henry, R. L. Pyrazine chemistry. IV. Bromination of 2-amino-3-carbomethoxypyrazine. *J. Am. Chem. Soc.* **1949**, *71*, 2798–800.

(29) Bonnefous, C.; Vernier, J.-M.; Hutchinson, J. H.; Chung, J.; Reyes-Manalo, G.; Kamenecka, T. Dipyridyl amides: Potent metabo-tropic glutamate subtype 5 (mGlu5) receptor antagonists. *Bioorg. Med. Chem. Lett.* **2005**, *15* (4), 1197–1200.

(30) Bonnefous, C.; Kamenecka, T.; Vernier, J.-M. Preparation of bipyridyl amides as modulators of metabotropic glutamate receptor-5; WO 2005079802.

(31) Yuan, J.; Guo, Q.; Zhao, H.; Hu, S.; Whitehouse, D.; Fringle, W.; Mao, J.; Maynard, G.; Hammer, J.; Wustrow, D.; Li, H. Preparation of substituted heteroaryl CB1 antagonists; WO 2006113704.

(32) Rushton, L.; Winter, J. J. G. Pyrazine derivatives as Axl and C-Met receptor enzyme inhibitors and their preparation and use in the treatment of tumors; WO 2009007390.

(33) Dunwell, D. W.; Evans, D.; Hicks, T. A. Synthesis and antiin-flammatory activity of some 2-heteroaryl-a -methyl-5-benzoxazoleacetic acids. *J. Med. Chem.* **1975**, *18* (11), 1158–1159.

(34) Sun, B.; Guan, J.-X.; Xu, L.; Yu, B.-L.; Jiang, L.; Kou, J.-F.; Wang, L.; Ding, X.-D.; Chao, H.; Ji, L.-N. DNA Condensation Induced by Ruthenium(II) Polypyridyl Complexes [Ru(bpy)2(PIPSH)]2+ and [Ru(bpy)2(PIPNH)]2. *Inorg. Chem.* **2009**, *48* (11), 4637–4639.

(35) Holljes, E. L., Jr.; Wagner, E. C. Some Reactions of Nitriles as Acid Anammonides. *J. Org. Chem.* **1944**, *9* (1), 31–49.

(36) Nakamura, H.; Takeuchi, D.; Murai, A. Synthesis of 5- and 3,5-substituted 2-aminopyrazines by Pd mediated Stille coupling. *Synlett* **1995**, *12*, 1227–1228. Adamczyk, M.; Akireddy, S. R.; Johnson, D. D.; Mattingly, P. G.; Pan, Y.; Reddy, R. E. Synthesis of 3,7-dihydroimidazo-[1,2a]pyrazine-3-ones and their chemiluminescent properties. *Tetrahedron* **2003**, *59* (41), 8129–8142.

(37) Ward, I. M.; Chen, J. Histone H2AX is phosphorylated in an ATR-dependent manner in response to replicational stress. *J. Biol. Chem.* **2001**, *276*, 47759–47762.

(38) Williams, R.; Berndt, A.; Miller, S.; Hon, W. C.; Zhang, X. Form and flexibility in phosphoinositide 3-kinases. *Biochem. Soc. Trans.* **2009**, *37* (4), 615–626.

(39) PDB entry 1E8Z: Walker, E. H.; Pacold, M. E.; Perisic, O.; Stephens, L.; Hawkins, P. T.; Wymann, M. P.; Williams, R. L. Structural determinants of phosphoinositide 3-kinase inhibition by wortmannin, LY294002, quercetin, myricetin, and staurosporine. *Mol. Cell* **2000**, *6* (4), 909–919.

(40) Sibanda, B. L.; Chirgadze, D. Y.; Blundell, T. L. Crystal structure of DNA-PKcs reveals a large open-ring cradle comprised of HEAT repeats. *Nature* **2010**, *463*, 118–122.

(41) Zhang, D.; Wang, Z.; Xu, W.; Sun, F.; Tang, L.; Wang, J. Design, synthesis and antibacterial activity of novel actinonin derivatives containing benzimidazole heterocycles. *Eur. J. Med. Chem.* **2009**, *44* (5), 2202–2210.

(42) Cheng, Y.; Prusoff, W. H. Relationship between the inhibition constant (K_i) and the concentration of inhibitor which causes 50% inhibition (I_{50}) of an enzymatic reaction. *Biochem. Pharmacol.* **1973**, *22*, 3099–3108.

(43) Cortez, D.; Guntuku, S.; Qin, J.; Elledge, S. J. ATR and ATRIP: partners in checkpoint signaling. *Science* **2001**, *294*, 1713–1716.

(44) Casper, A. M.; Nghiem, P.; Arlt, M. F.; Glover, T. W. ATR regulates fragile site stability. *Cell* **2002**, *111*, 779–789.

(45) Sorensen, C. S.; Syljuasen, R. G.; Lukas, J.; Bartek, J. ATR, Claspin and the Rad9-Rad1-Hus1 complex regulate Chk1 and Cdc25A in the absence of DNA damage. *Cell Cycle* **2004**, *3*, 941–945.

(46) Hurley, P. J.; Wilsker, D.; Bunz, F. Human cancer cells require ATR for cell cycle progression following exposure to ionizing radiation. *Oncogene* **2007**, *26*, 2535–2542.

(47) Wilsker, D.; Bunz, F. Loss of ataxia telangiectasia mutated- and Rad3-related function potentiates the effects of chemotherapeutic drugs on cancer cell survival. *Mol. Cancer Ther.* **2007**, *6*, 1406–1413.

(48) Cliby, W. A.; Roberts, C. J.; Cimprich, K. A.; Stringer, C. M.; Lamb, J. R.; Schreiber, S. L.; Friend, S. H. Overexpression of a kinase-inactive ATR protein causes sensitivity to DNA-damaging agents and defects in cell cycle checkpoints. *EMBO J.* **1998**, *17*, 159–169.

(49) Kim, W. J.; Vo, Q. N.; Shrivastav, M.; Lataxes, T. A.; Brown, K. D. Aberrant methylation of the ATM promoter correlates with increased radiosensitivity in a human colorectal tumor cell line. *Oncogene* **2002**, *21*, 3864–3871.

(50) Takemura, H; Rao, V. A.; Sordet, O.; Furuta, T.; Miao, Z.-H.; Meng, L.; Zhang, H.; Pommier, Y. Defective Mre11-dependent activation of Chk2 by ataxia telangiectasia mutated in colorectal carcinoma cells in response to replication-dependent DNA double strand breaks. *J. Biol. Chem.* **2006**, *281*, 30814–30823.

(51) Prichard, M. N.; Prichard, L. E.; Shipman, C., Jr. Strategic design and three-dimensional analysis of antiviral drug combinations. *Antimicrob. Agents Chemother.* **1993**, *37*, 540–545.

(52) Unsal-Kaçmaz, K.; Makhov, A. M.; Griffith, J. D.; Sancar, A. Preferential binding of ATR protein to UV-damaged DNA. *Proc. Natl. Acad. Sci. U.S.A.* **2002**, *99*, 6673–6678.

(53) Pitt, A. M.; Lee, C. High throughput screening protein kinase assays optimized for reaction, binding, and detection totally within a 96-well plate. *J. Biomol. Screening* **1996**, *1*, 47–51.